optica

Volume 4 • Issue 1 • January 2017

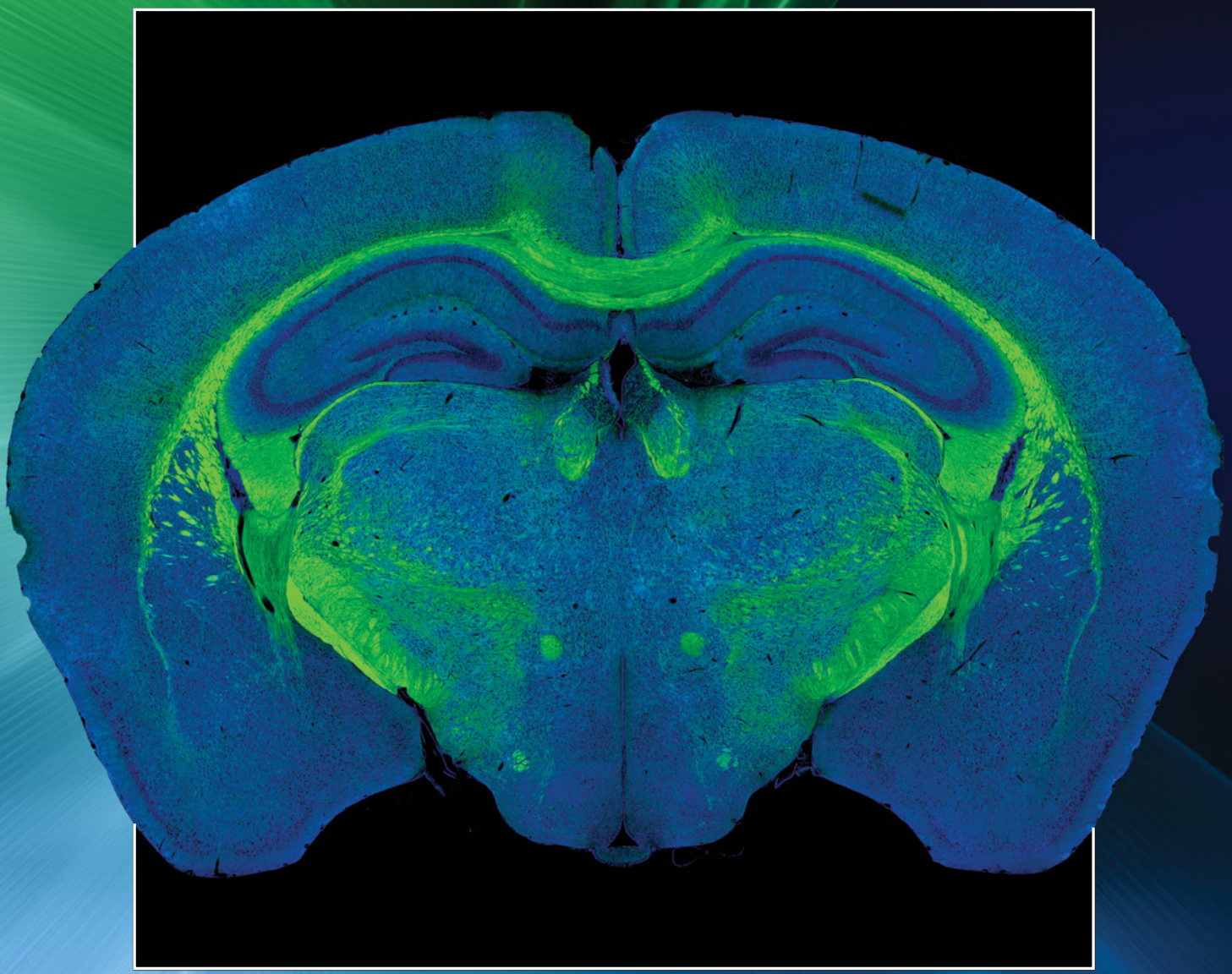

OSA®
The Optical Society

ISSN: 2334-2536

optica.osa.org

optica

Dual-phase stimulated Raman scattering microscopy for real-time two-color imaging

Ruoyu He,[1] Yongkui Xu,[1] Lili Zhang,[1] Shenghong Ma,[2,3] Xu Wang,[2] Dan Ye,[2,3,4] and Minbiao Ji[1,4,*]

[1]State Key Laboratory of Surface Physics and Department of Physics, Fudan University, Shanghai 200433, China
[2]Key Laboratory of Metabolism and Molecular Medicine, Ministry of Education, and Department of Biochemistry and Molecular Biology, School of Basic Medical Sciences, Fudan University, Shanghai 200032, China
[3]State Key Laboratory of Genetic Engineering, Molecular and Cell Biology Lab, Institute of Biomedical Sciences, Shanghai Medical College, Fudan University, Shanghai 200032, China
[4]Collaborative Innovation Center of Genetics and Development, School of Life Sciences, Fudan University, Shanghai 200433, China
*Corresponding author: minbiaoj@fudan.edu.cn

Received 8 August 2016; revised 31 October 2016; accepted 30 November 2016 (Doc. ID 273451); published 22 December 2016

Label-free histology with chemical contrast has great potential for rapid intraoperative diagnosis. Two-color stimulated Raman scattering (SRS) microscopy has shown success in label-free digital histology with diagnostic results similar to those of hematoxylin and eosin stain. However, achieving real-time two-color SRS imaging has been a challenge. We have precisely engineered the pulse profiles of Stokes beams, and fully utilized in-phase (X) and quadrature (Y) outputs of a phase-sensitive lock-in amplifier to realize simultaneous two-color imaging. Such a method could reach the maximum speed as in single-color SRS, and has proven its robustness and advantages in real-time histology as well as *in vivo* imaging of live animals, both in transmission and epi modes. Moreover, this method could be conveniently adapted to other pump–probe-based microscopes.

OCIS codes: (220.4830) Systems design; (170.0110) Imaging systems; (290.5910) Scattering, stimulated Raman; (170.5660) Raman spectroscopy.

https://doi.org/10.1364/OPTICA.4.000044

As one of the coherent Raman scattering (CRS) imaging techniques, stimulated Raman scattering (SRS) microscopy has demonstrated unique capabilities in quantitative chemical analysis, live cell drug delivery, DNA imaging, and tumor detection [1–9]. The major advantages of SRS reside in its high sensitivity and chemical specificity without the need for any exogenous labeling. On one hand, SRS inherits vibrational spectroscopy from spontaneous Raman scattering, with intrinsic molecular markers from the "fingerprint" spectral features. On the other hand, its nonlinear and coherent optical process amplifies the Raman signal by 3–5 orders of magnitude, enabling fast imaging and sensitive detection. Consequently, achieving better spectroscopy and a higher imaging rate has been a long-term pursuit in the field [10,11]. However, it is difficult to have both. Single-color CRS has reached the highest imaging speed (up to video rate), but it sacrificed spectral information and chemical resolution [12–14]. At the other extreme, hyperspectral SRS and broadband coherent anti-Stokes Raman scattering managed to cover a wide spectral range with fine spectral resolution, but at the cost of more pixel integration time [15–21].

SRS spectral imaging techniques could be divided into two major categories: sequential and parallel methods. Sequential methods rely on wavelength sweeping techniques with narrowband lasers, including mechanical [4,22,23] and electro-optical means of wavelength selection [24,25], but their speeds are limited due to the inevitable time consumption associated with wavelength tuning. Parallel methods incorporate broadband lasers, and can be further split into two types: dispersive detection and modulation multiplexing techniques. Dispersive detection methods are based on a spectrometer setting with array detectors and demodulators [26–28], which are limited to imaging thin samples in transmission mode. Modulation multiplexing techniques involve a spectrally modulated broadband excitation beam and a point detector, followed by Fourier transformation to obtain spectral information [9,29], but the highest imaging rate to date is ~60 μs/pixel. Other methods including spectrally tailored excitation SRS [30] and Fourier transform SRS [31] have also been demonstrated, but they are largely limited by their complexity and speed. Despite these efforts, real-time histological imaging with multichemical contrast has never been achieved in live animals in epi mode, which is a key step for the clinical translation of SRS microscopy.

We have previously demonstrated the potential of two-color SRS microscopy as a label-free histological tool to delineate tumor from normal tissues [5,32]. Compared with single-color imaging, two-color SRS provides much better contrast of cell density, nuclear morphology, axon density, etc., generating diagnostic results similar to the hematoxylin and eosin (H&E) stain method, which is widely used as the gold standard in histology. In a way, H&E could also be viewed as a two-color imaging modality, with hematoxylin and eosin labeling DNA and protein, respectively. The major advantage of SRS over H&E is its capability of imaging fresh, unprocessed tissues, thus potentially serving as a rapid label-free histology tool for *in vivo* diagnosis without biopsy. To achieve this goal, its imaging speed needs to be maximized with two-color contrast.

In this work, we present a compact design of parallel two-color SRS microscopy with the two orthogonal outputs of a dual-phase

lock-in amplifier (LIA). The experimental setup is illustrated in Fig. 1, which is based on a spectral focusing geometry [4,15,33]. Briefly, pulsed femtosecond laser beams from a commercial optical parametric oscillator (Insight DS+) were used to serve as the Stokes (1040 nm, ~150 fs) and pump (690–1300 nm, ~120 fs) beam. The pulses were linearly chirped through highly dispersive SF57 glass rods, and the target Raman frequency could be conveniently selected by adjusting the relative time delay τ between the pump and Stokes pulses [Figs. 1(a) and 1(b)] with an optical delay line (DL1). The Stokes beam was modulated by an electro-optical modulator followed by a polarizing beam splitter (PBS1), and the transmitted Stokes beam (S_1) was collinearly combined with the pump beam through a dichroic mirror. Then both beams were delivered to a laser scanning microscope (FV1200, Olympus) and interacted with the samples. Finally, the stimulated Raman loss (SRL) signal in the pump beam was filtered and demodulated by an LIA (HF2LI, Zurich Instruments) to form SRS images.

A dual-path SRS setup was built upon the above apparatus with precise temporal control. First, the modulation frequency was locked to 1/4 the laser pulse repetition rate ($f_0 = 80$ MHz); thus each modulation period contains exactly four pulse intervals. Second, the Stokes beam reflected by PBS1 was recycled to serve as a second Stokes beam (S_2), which was recombined with S_1 at PBS2 after another optical delay line (DL2). Notice that S_1 and S_2 were modulated in antiphase right after PBS1, but this phase difference was altered after PBS2 based on the amount of delay in DL2. As can be seen, the combination of DL1 and DL2 fully controls the delay profiles of the two Stokes beams at τ_1 and τ_2, which correspond to the target Raman frequencies of Ω_1 and Ω_2. The essential part of the design was to add one pulse interval T_0 ($1/f_0 = 12.5$ ns) to DL2, so that the time delay between S_1 and S_2 became $T_0 + \Delta\tau$. Such a temporal design achieves two critical goals: first, adding T_0 in S_2 effectively shifts the phase difference between S_1 and S_2 from π to $\pi/2$ without affecting the SRS signal strength [Fig. 1(c)]; second, the fine adjustment of $\Delta\tau$ determines the probe Raman frequencies at Ω_1 and Ω_2. Also, notice that $\Delta\tau$ was only a few picoseconds, which makes for a negligible phase change ($\Delta\tau/T_0 \sim 10^{-4}$). In the end, the SRL signals at frequency Ω_1 and Ω_2 were generated in the pump beam with a $\pi/2$ phase difference, which could be written as

$$I_{\mathrm{SRL}}(t) = I(\Omega_1)\,\sin\left(\frac{\pi f_0 t}{2} + \phi_0\right) + I(\Omega_2)\,\cos\left(\frac{\pi f_0 t}{2} + \phi_0\right). \quad (1)$$

Therefore, a phase-sensitive LIA could be used to detect $I(\Omega_1)$ and $I(\Omega_2)$ simultaneously through the in-phase (X) and quadrature (Y) output channels with proper setting of the reference phase ϕ_0.

Two major potential issues need to be addressed in this design. First, there is the optical interference between the S_1 and S_2 beams, which could cause significant fluctuations in SRS signals. Second, there is electronic cross talk between the X and Y channels of the LIA, which would lead to spectral artifacts when applying numerical decomposition to extract different chemical components [9]. We tested the interference effect with a Michelson interferometer for laser beams under a varying amount of chirp. As expected, although the insertion of glass rods expands the pulse duration due to group velocity dispersion, the coherence time remains unchanged (see Fig. S1 of Supplement 1). The interferogram and autocorrelation of the laser beams are presented in Fig. 2(a), showing a pulse duration of 1.8 ps and coherence time of ~250 fs for the Stokes beam. The measured duration of the pump pulse was 3.8 ps. Probing the Raman frequency at 2848 and 2926 cm^{-1} for lipid/protein imaging, the relative time delay was found to be $\Delta\tau = 2.3$ ps, which was almost 10 times as large as the coherence time. Under such a condition, the interference effect was vanishingly small, as seen in our results. In fact, the setup was stable enough for $\Delta\tau > 1$ ps, i.e., $\Delta\Omega > 36$ cm^{-1}, which is slightly larger than the spectral resolution of our system (~23 cm^{-1}; see Fig. S2 of Supplement 1). The cross talk between the two channels was investigated in detail using the acquired SRS spectra and images shown below.

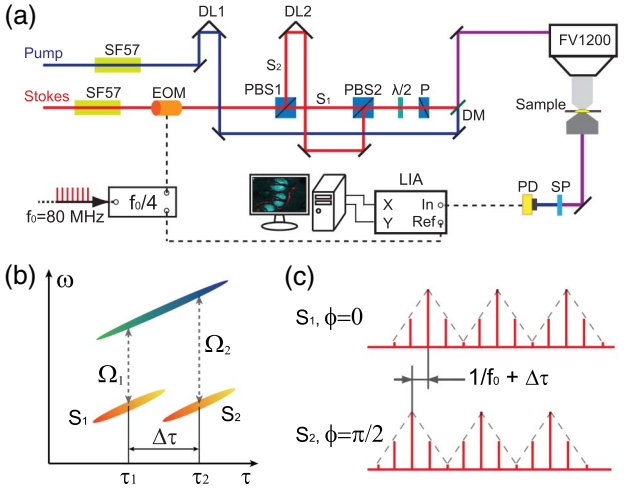

Fig. 1. System design of the dual-phase SRS microscope. (a) Optical layout of the setup. DL, delay line; EOM, electro-optical modulator; PBS, polarizing beam splitter; $\lambda/2$, half-wave plate; P, polarizer; DM, dichroic mirror; SP, short pass filter; PD, photodiode; LIA, lock-in amplifier. (b) Schematic chirp and temporal profiles of the pump (blue) and two Stokes beams (orange) in the spectral focusing setting. S_1 and S_2 with time delay τ_1 and τ_2 correspond to the SRS signals at frequencies Ω_1 and Ω_2, respectively. (c) Pulse trains of the modulated S_1 and S_2, showing the modulation phase difference.

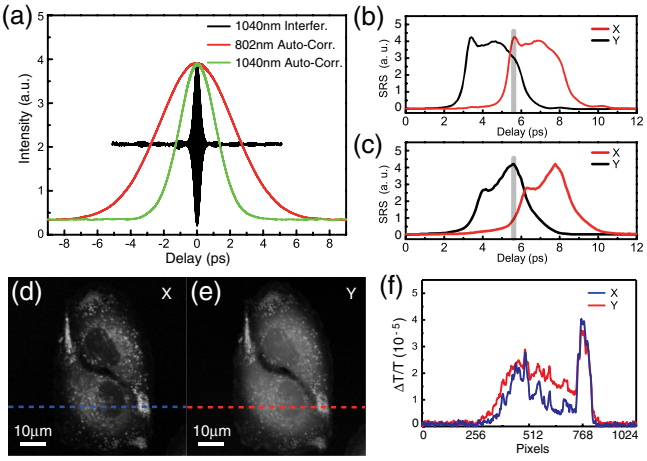

Fig. 2. Validation of the system performance. (a) Interferogram of the Stokes beam and autocorrelation of the pump and Stokes beams. Simultaneous SRS spectra of (b) oleic acid and (c) bovine serum albumin from the X and Y channels of LIA. The gray bar indicates the delay position of DL1 to simultaneously image A549 cells at (d) 2848 cm^{-1} in the X channel and (e) 2926 cm^{-1} in the Y channel (1024 × 1024 pixels, 2 μs/pixel, with 60X objective). (f) Line profiles of the signal distributions in (d) and (e).

We first evaluated the system by acquiring SRS spectra for standard test chemicals: oleic acid and bovine serum albumin. SRS spectra from the X and Y channels were recorded simultaneously by scanning DL1 while keeping DL2 fixed to ensure $\Delta\tau = 2.3$ ps. The reference phase of the LIA was optimized to minimize the cross talk between the X and Y channels, as can be seen from the vanishing signal in the X (Y) channel when its corresponding Stokes beam S_1 (S_2) was blocked (see Fig. S3 of Supplement 1). When both beams were open, almost identical spectra from the two output channels were generated with little distortion [Figs. 2(b) and 2(c)], indicating negligible cross talk or interference when probing SRS without beam scanning.

Next we imaged live cells in transmission mode. With beam scanning, the detected laser spot moves across the large photodiode (PD), which might cause a change in the RF phase and generate spatially dependent cross talk. To minimize such an effect, we placed the PD at the image plane of the pupil of the condenser, where the beam spot was large and had minimal movement. We evaluated the cross talk with cultured A549 cells by varying the position of the DL1 under fixed $\Delta\tau = 2.3$ ps when acquiring dual-phase SRS images. More detailed analysis was shown in Fig. S4 of Supplement 1, indicating the amplitude of the cross talk to be ~2%. When the delay of DL1 was set properly [gray bars in Figs. 2(b) and 2(c)], dual-phase SRS could probe 2848 and 2926 cm^{-1} simultaneously, as shown in Figs. 2(d) and 2(e), where the distributions of intracellular lipids and proteins are clearly shown; the line profiles are plotted in Fig. 2(f).

Such a parallel detection method has a major advantage in reducing imaging time, especially when dealing with large samples such as tissue sections. We performed dual-phase SRS imaging on mouse brain coronal sections. Our results replicated previous images taken by sequential wavelength tuning [5,32], but in less than 50% of the total imaging time (~30 min). All the detailed brain structures, as well as lipid (green) and protein (blue) distributions, are clearly displayed in Fig. 3. Histological features based on cell morphologies and densities are readily seen and can be used for diagnosis, as reported previously [5,32]. The cross-talk amplitude of the transmission mode tissue imaging was found to be similar to that of the cell imaging mode. We also provide real-time histology for simulated on-site diagnosis during slide scanning (Visualization 1). These results indicate the potential of our method for rapid label-free histology.

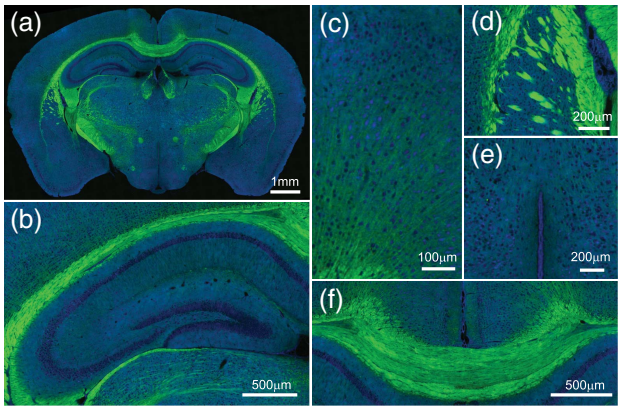

Fig. 3. Simultaneous two-color SRS images of mouse brain sections. Lipids are false-colored green, with proteins in blue. (a) Full coronal section, composed via tiling of 17 × 27 frames (512 × 512 pixels, 2 μs/pixel, with 25X objective), (b) hippocampus, (c) cortex, (d) caudatoputamen, (e) hypothalamic nuclei, (f) corpus callosum.

Our dual-phase SRS technique provides an optimum tool for *in vivo* imaging. Its parallel nature eliminates motion artifacts [9,24] that were almost inevitable in all sequential multicolor imaging methods (see Fig. S5 of Supplement 1). In principle, it could reach the highest imaging speed used in single-color SRS. We imaged live animals in transmission mode, aiming at simultaneous mapping of hemoglobin and protein contents, whose spectra were shown in Fig. S6 of Supplement 1. The heartbeats of zebrafish embryos (5 days after fertilization) were recorded with a pixel dwell time of 500 ns (the shortest of our system) and imaging rate of 8 frames/s. As shown in Fig. 4(a) and Visualization 2, we observed the fast-moving oval-shaped blood cells flowing in and out of the zebrafish hearts, and the localized hemoglobin at the early developmental stage [34,35]. We also captured blood streams in mouse ears in real time [Fig. 4(b) and Visualization 3 and Visualization 4], where individual red blood cells could be clearly visualized. These results proved the robustness of our method in imaging fast-moving objects, without any detectable motion artifacts or cross talk.

We further validated our method for live animal imaging in epi mode, using a specially designed annular detector to collect the backscattered photons [5,32]. In our scheme, the laser beams pass through the central hole of the PD and filter, and are focused onto the sample and diffused into the tissues. The backscattered photons harvested by the PD form a large spot, the motion and shape change of which were expected to be small during beam scanning or focal depth changing (within 100 μm). As shown in Fig. 4(c) (and in Fig. S7 of Supplement 1), *in vivo* two-color images of the mouse skin were taken at different depths, showing lipid/protein profiles of the stratum corneum, sebaceous gland, and adipocytes. The cross talk was found to be less than 4% throughout the imaging depth [Fig. 4(d)], although the decreased SNR (from ~50 to ~10) caused larger uncertainties in the measurements. The

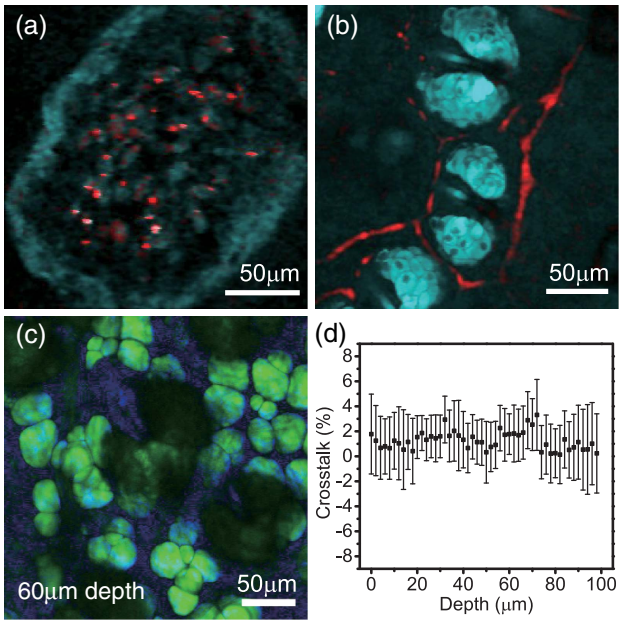

Fig. 4. *In vivo* two-color SRS microscopy images of live animals. Real-time images of hemoglobin (red) and protein (cyan) in transmission mode, including (a) the heart of a zebrafish embryo and (b) blood streams in a mouse ear; (c) epi mode SRS of the subcutaneous adipocytes in a live mouse ear, with lipids (green) and protein (blue) distributions (256 × 256 pixels, 0.5 μs/pixel, 25X objective); (d) the magnitude of cross talk at various imaging depths.

success of our method in epi mode demonstrates great potential for its application in label-free intraoperative imaging and diagnosis.

All previous methods for SRS spectral imaging were considered to be frequency domain techniques, either in the optical frequency domain, such as wavelength sweeping [4,22,24,25] and dispersive detection [26], or in the RF domain with modulation multiplexing [9,26]. The underlying principle has been based on the orthogonality between Fourier components of different frequencies. In contrast, our method utilized the orthogonality between sine and cosine functions, and opened up a new route for extracting spectral information. It is also possible to combine such a concept with existing frequency domain methods to further improve the imaging speed of multicolor SRS.

The simplicity of our design enables its easy maintenance and flexibility. For example, we could immediately go back to a normal SRS setup by simply blocking the S_2 beam. And if we reduce DL2 by T_0 so that S_1 and S_2 are modulated in antiphase, it becomes a frequency-modulation (FM) SRS system, detecting the differential signal $I(\Omega_1) - I(\Omega_2)$, although FM-SRS is essentially a single-color imaging system. Once our dual-phase setup is optimized, there is no need to tune the laser wavelength or move any mechanical part during image acquisition, and thus superior stability and durability could be expected.

In addition to rapid histology and intraoperative imaging, more potential applications could be found to favor our method. For instance, various biomedical problems that involve flow systems, such as lipid/protein-based cell analysis and sorting on the platform of flow cytometry [36]; hematology in zebrafish and other animals [34,37]; and *in vivo* detection of circulating tumor cells [38]. Last but not least, this method could be readily applied to other pump–probe-based microscopes to image two components simultaneously, provided that they have distinct transient behaviors [37,39,40].

In summary, we have designed a compact two-color SRS microscope with precise temporal engineering that is capable of detecting two Raman frequencies simultaneously through the in-phase and quadrature output channels of a dual-phase LIA. We have demonstrated the proof-of-principle results in imaging cultured cells, tissue sections, and live animals, in both transmission and epi modes. Our approach provides a convenient way to achieve real-time two-color SRS imaging, and could find new possibilities in biomedical research.

Funding. National Key Research and Development project (2016YFC0102100); Shanghai Rising Star program (15QA1400500); Shanghai Action Plan for Scientific and Technological Innovation program (16441909200); National Natural Science Foundation of China (NSFC) (81671725).

See Supplement 1 for supporting content.

REFERENCES

1. C. W. Freudiger, W. Min, B. G. Saar, S. Lu, G. R. Holtom, C. He, J. C. Tsai, J. X. Kang, and X. S. Xie, Science **322**, 1857 (2008).
2. E. Ploetz, S. Laimgruber, S. Berner, W. Zinth, and P. Gilch, Appl. Phys. B **87**, 389 (2007).
3. M. C. Wang, W. Min, C. W. Freudiger, G. Ruvkun, and X. S. Xie, Nat. Methods **8**, 135 (2011).
4. D. Fu, Y. Yu, A. Folick, E. Currie, R. V. Farese, Jr., T. H. Tsai, X. S. Xie, and M. C. Wang, J. Am. Chem. Soc. **136**, 8820 (2014).
5. M. Ji, D. A. Orringer, C. W. Freudiger, S. Ramkissoon, X. Liu, D. Lau, A. J. Golby, I. Norton, M. Hayashi, N. Y. Agar, G. S. Young, C. Spino, S. Santagata, S. Camelo-Piragua, K. L. Ligon, O. Sagher, and X. S. Xie, Sci. Transl. Med. **5**, 201 (2013).
6. L. Wei, F. Hu, Y. Shen, Z. Chen, Y. Yu, C. C. Lin, M. C. Wang, and W. Min, Nat. Methods **11**, 410 (2014).
7. S. Hong, T. Chen, Y. Zhu, A. Li, Y. Huang, and X. Chen, Angew. Chem. **53**, 5827 (2014).
8. D. Zhang, P. Wang, M. N. Slipchenko, D. Ben-Amotz, A. M. Weiner, and J. X. Cheng, Anal. Chem. **85**, 98 (2013).
9. F. Dan, F. K. Lu, Z. Xu, C. Freudiger, D. R. Pernik, G. Holtom, and X. S. Xie, J. Am. Chem. Soc. **134**, 3623 (2012).
10. J. X. Cheng and X. S. Xie, Science **350**, aaa8870 (2015).
11. C. Chung, J. Boik, and E. O. Potma, Ann. Rev. Phys. Chem. **64**, 77 (2013).
12. A. Zumbusch, G. R. Holtom, and X. S. Xie, Phys. Rev. Lett. **82**, 4142 (1999).
13. C. L. Evans, E. O. Potma, M. Puoris'haag, D. Cote, C. P. Lin, and X. S. Xie, Proc. Natl. Acad. Sci. USA **102**, 16807 (2005).
14. B. G. Saar, C. W. Freudiger, J. Reichman, C. M. Stanley, G. R. Holtom, and X. S. Xie, Science **330**, 1368 (2010).
15. D. Fu, G. Holtom, C. Freudiger, X. Zhang, and X. S. Xie, J. Phys. Chem. B **117**, 4634 (2013).
16. C. H. Camp, Jr., Y. J. Lee, J. M. Heddleston, C. M. Hartshorn, A. R. H. Walker, J. N. Rich, J. D. Lathia, and M. T. Cicerone, Nat. Photonics **8**, 627 (2014).
17. K. Hashimoto, M. Takahashi, T. Ideguchi, and K. Goda, Sci. Rep. **6**, 21036 (2016).
18. T. Hellerer, A. M. K. Enejder, and A. Zumbusch, Appl. Phys. Lett. **85**, 25 (2004).
19. A. F. Pegoraro, A. Ridsdale, D. J. Moffatt, Y. Jia, J. P. Pezacki, and A. Stolow, Opt. Express **17**, 2984 (2009).
20. E. R. Andresen, P. Berto, and H. Rigneault, Opt. Lett. **36**, 2387 (2012).
21. I. Rocha-Mendoza, W. Langbein, and P. Borri, Appl. Phys. Lett. **93**, 201103 (2008).
22. F. K. Lu, S. Basu, V. Igras, M. P. Hoang, M. Ji, D. Fu, G. R. Holtom, V. A. Neel, C. W. Freudiger, and D. E. Fisher, Proc. Natl. Acad. Sci. USA **112**, 11624 (2015).
23. Y. Ozeki, W. Umemura, Y. Otsuka, S. Satoh, H. Hashimoto, K. Sumimura, N. Nishizawa, K. Fukui, and K. Itoh, Nat. Photonics **6**, 845 (2012).
24. L. Kong, M. Ji, G. R. Holtom, F. Dan, C. W. Freudiger, and X. X. Sunney, Opt. Lett. **38**, 145 (2013).
25. S. Karpf, M. Eibl, W. Wieser, T. Klein, and R. Huber, Nat. Commun. **6**, 6784 (2015).
26. F. Lu, M. Ji, D. Fu, X. Ni, C. W. Freudiger, G. Holtom, and X. S. Xie, Mol. Phys. **110**, 1927 (2012).
27. C. Liao, M. N. Slipchenko, P. Wang, J. Li, S. Y. Lee, R. A. Oglesbee, and J. Cheng, Light: Sci. Appl. **4**, e265 (2015).
28. K. Seto, Y. Okuda, E. Tokunaga, and T. Kobayashi, Rev. Sci. Instrum. **84**, 083705 (2013).
29. C. Liao, P. Wang, P. Wang, J. Li, H. J. Lee, G. Eakins, and J. Cheng, Sci. Adv. **1**, e1500738 (2015).
30. C. W. Freudiger, W. Min, G. R. Holtom, B. Xu, M. Dantus, and X. S. Xie, Nat. Photonics **5**, 103 (2011).
31. J. Réhault, F. Crisafi, V. Kumar, G. Ciardi, M. Marangoni, G. Cerullo, and D. Polli, Opt. Express **23**, 25235 (2015).
32. M. Ji, S. Lewis, S. Camelo-Piragua, S. H. Ramkissoon, M. Snuderl, S. Venneti, A. Fisher-Hubbard, M. Garrard, D. Fu, A. C. Wang, J. A. Heth, C. O. Maher, N. Sanai, T. D. Johnson, C. W. Freudiger, O. Sagher, X. S. Xie, and D. A. Orringer, Sci. Transl. Med. **7**, 309ra163 (2015).
33. S. Funkner, K. Saito, G. Niehues, Y. Yazawa, T. Furuya, K. Yamamoto, and M. Tani, Appl. Phys. Lett. **105**, 021103 (2014).
34. D. Carradice and G. J. Lieschke, Blood **111**, 3331 (2008).
35. J. M. Murtha, W. Qi, and E. T. Keller, Comp. Med. **53**, 37 (2003).
36. W. He, H. Wang, L. C. Hartmann, J. X. Cheng, and P. S. Low, Proc. Natl. Acad. Sci. USA **104**, 11760 (2007).
37. D. Fu, T. Ye, T. E. Matthews, B. J. Chen, G. Yurtserver, and W. S. Warren, Opt. Lett. **32**, 2641 (2007).
38. M. Zhong, X. Wei, J. Zhou, Z. Wang, and Y. Li, Nat. Commun. **4**, 1768 (2013).
39. W. Min, S. Lu, S. Chong, R. Roy, G. R. Holtom, and X. S. Xie, Nature **461**, 1105 (2009).
40. T. E. Matthews, I. R. Piletic, M. A. Selim, M. J. Simpson, and W. S. Warren, Sci. Transl. Med. **3**, 71ra15 (2011).